Int. J. Heat Mass Transfer. Vol. 26, No. 12, pp. 1867–1878, 1983
Printed in Great Britain

0017-9310/83 $3.00 + 0.00

NATURAL CONVECTION IN A PARTIALLY DIVIDED ENCLOSURE

NIENCHUAN N. LIN and ADRIAN BEJAN
Department of Mechanical Engineering, Campus Box 427, University of Colorado, Boulder, CO 80309, U.S.A.

(*Received* 16 *November* 1982 *and in revised form* 14 *April* 1983)

Abstract—This paper describes an experimental and analytical study of the phenomenon of heat transfer by natural convection in a rectangular enclosure fitted with an incomplete internal partition. The experiments were carried out in a water-filled enclosure with adiabatic horizontal walls and vertical walls maintained at different temperatures. Heat transfer measurements and flow visualization studies were conducted in the Rayleigh number range 10^9–10^{10}, for aperture ratios $h/H = 1, 1/4, 1/8, 1/16$, and 0, where h and H are the height of the internal opening (above the partition) and the height of the enclosure, respectively. It is demonstrated that the aperture ratio h/H has a strong effect on both the heat transfer rate and the flow pattern. The second part of the study consists of an asymptotic analysis of the same phenomenon, valid in the limit of vanishing Rayleigh numbers. The flow and temperature fields in this limit are reported graphically for $H/L = 0.5$, $Pr = 0.71$ and $0.3 < h/H < 0.7$, where L and Pr are the enclosure length and the Prandtl number, respectively.

NOMENCLATURE

A	aspect ratio, H/L
Ap	aperture ratio, h/H
g	acceleration due to gravity
h	distance from enclosure ceiling to partition (aperture height)
H	enclosure height
k	thermal conductivity
L	enclosure length
Nu	Nusselt number, $(Q/W)/[k(T_H - T_C)]$
Pr	Prandtl number, ν/α
Q	heat transfer across enclosure
R_C	thermal resistance lining the cold wall
R_H	thermal resistance lining the hot wall
Ra_H	Rayleigh number based on enclosure height H
Ra_L	Rayleigh number based on enclosure length L
T	temperature [°C]
T_H	warm end temperature
T_C	cold end temperature
ΔT	temperature difference between the hot and cold wall
u	horizontal velocity
v	vertical velocity
W	enclosure width
x, y	Cartesian coordinates
X, Y	dimensionless Cartesian coordinates, x/L, y/L.

Greek symbols

α	thermal diffusivity
β	coefficient of thermal expansion
θ	dimensionless temperature, $(T - T_C)/(T_H - T_C)$
ν	kinematic viscosity
ζ	vorticity
Z	dimensionless vorticity, $\zeta/[\beta g L(T_H - T_C)/\nu]$
ψ	stream function
Ψ	dimensionless stream function, $\psi/[\beta g L^3(T_H - T_C)/\nu]$.

Subscripts

C	cold wall
H	hot wall.

1. INTRODUCTION

THE PHENOMENON of heat transfer by natural convection in enclosures heated from the side has attracted considerable interest during the past decade [1–3]. To a large extent, this interest is stimulated by the contemporary emphasis placed on the need to design energy-efficient buildings as well as efficient solar energy installations. As summarized in refs. [1–3], the bulk of heat transfer research on natural convection in enclosures has been devoted to enhancing man's understanding of what can happen in a 'single' enclosure: the most frequently used model in the existing studies consists of a rectangular two-dimensional enclosure with heating and cooling administered along the two opposing vertical walls.

Although much remains to be done to understand this basic model, especially its high Rayleigh number behavior and the influence of lateral walls (three-dimensional effects), it is evident that real-life systems such as buildings and solar collectors only rarely conform to the 'single enclosure' description. The need to rethink our modeling of natural convection in enclosures was highlighted in the conclusions to the 1982 NSF Natural Convection Workshop [4]: It has been pointed out that a very basic configuration for the study of natural convection in buildings is the 'association' of two enclosures which communicate laterally through an opening in the same manner as two rooms connected through a doorway, window, corridor or over an incomplete dividing wall. This

'partially-divided enclosure' model is relatively unknown, in fact, we are aware of only three fundamental studies in which the phenomenon was investigated in the laboratory [5–7].

The object of the present study is to shed more light on the fluid mechanics and heat transfer characteristics of a partially divided enclosure heated from the side (Fig. 1). To understand the specific objectives of the present study, it is worth reviewing the main conclusions furnished by the preceding investigations [5–7]. Bejan and Rossie [5] described a water experiment in which two differentially-heated chambers exchanged heat through a short duct connecting the two chambers. The connecting duct was situated at mid-height. Flow visualization experiments and velocity measurements showed that the fluid becomes 'trapped' on both sides of the opening, cold fluid in the lower half of the cold chamber and warm fluid in the upper half of the hot chamber. Heat transfer measurements and scaling analysis showed that the heat transfer rate is dictated by the height of the opening relative to the differentially heated side walls; at the same time, it was argued that the heat transfer rate is independent of the length of the connecting duct.

Nansteel and Greif [6] studied an even more basic configuration, namely, the set-up of Fig. 1 where the enclosure is partially divided by a vertical incomplete wall. They used water in a briefcase-size apparatus and discovered a similar 'fluid trap' effect whereby the fluid stagnates on the upper-warm side of the partition (in ref. [6], the partition was attached to the upper wall, which is the same as rotating Fig. 1 by 180°). Heat transfer measurements showed conclusively that the heat transfer rate decreases as the opening h (or the aperture ratio $Ap = h/H$) decreases. Nansteel and Greif used two different partition materials (aluminum and polystyrene foam clad with stainless steel sheets) which, for reasons made clear later in the present study, can be described as 'more conducting' and 'less conducting'. The heat transfer measurements showed that the heat transfer reduction caused by decreasing Ap from 1 to 1/4 is most pronounced in the case of the 'less conducting' partition.

Most recently, Bajorek and Lloyd [7] described a series of experiments in a square enclosure with two partial dividers, one attached to the top wall and the other to the bottom. This arrangement amounts to two chambers communicating through a mid-height window, an arrangement similar to that of ref. [5]. However, unlike in refs [5, 6] where the working fluid was water and $Ra = O(10^{10})$, Bajorek and Lloyd used air and CO_2 and their Rayleigh numbers were considerably lower, $O(10^6)$. Comparing the heat transfer measurements taken in the partitioned enclosure with the corresponding measurements in the unpartitioned (single) enclosure, Bajorek and Lloyd found that the partitions reduce the heat transfer rate appreciably. Mach–Zehnder interferograms showed that the partitions have a noticeable impact on the isotherm pattern, however, ref. [7] does not contain flow visualization experiments or velocity measurements to complement the interferograms.

In view of what has already been contributed by refs. [5–7], the present study focuses on the most elementary configuration of ref. [6], Fig. 1, and seeks to:

(1) visualize the flow field in a more quantitative way than the dye-injection method of ref. [6];

(2) measure the fluid velocity in important places (e.g. the opening above the partial divider), as such measurements are presently unavailable, yet they can serve to verify the validity of high-Ra numerical simulations of the same flow [8];

(3) extend the heat transfer measurements to the

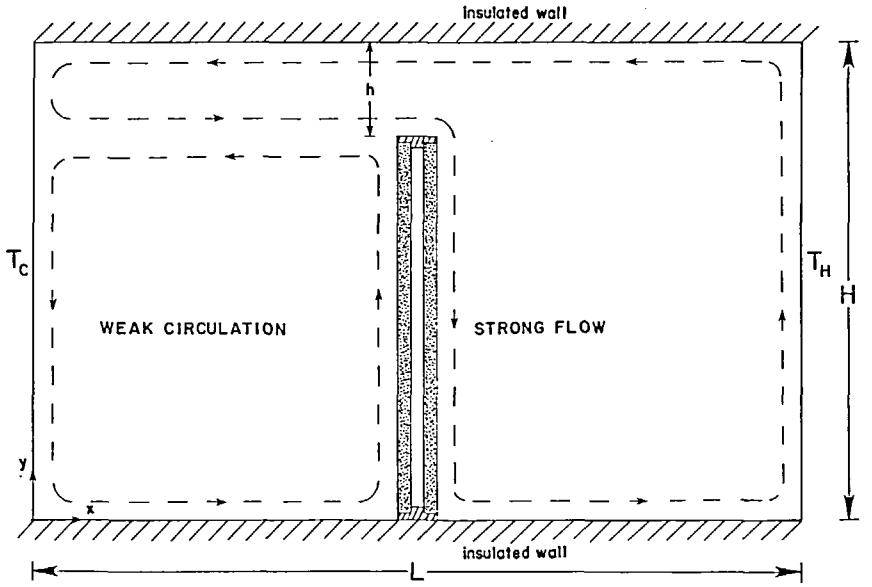

FIG. 1. Schematic of partially divided enclosure and flow pattern.

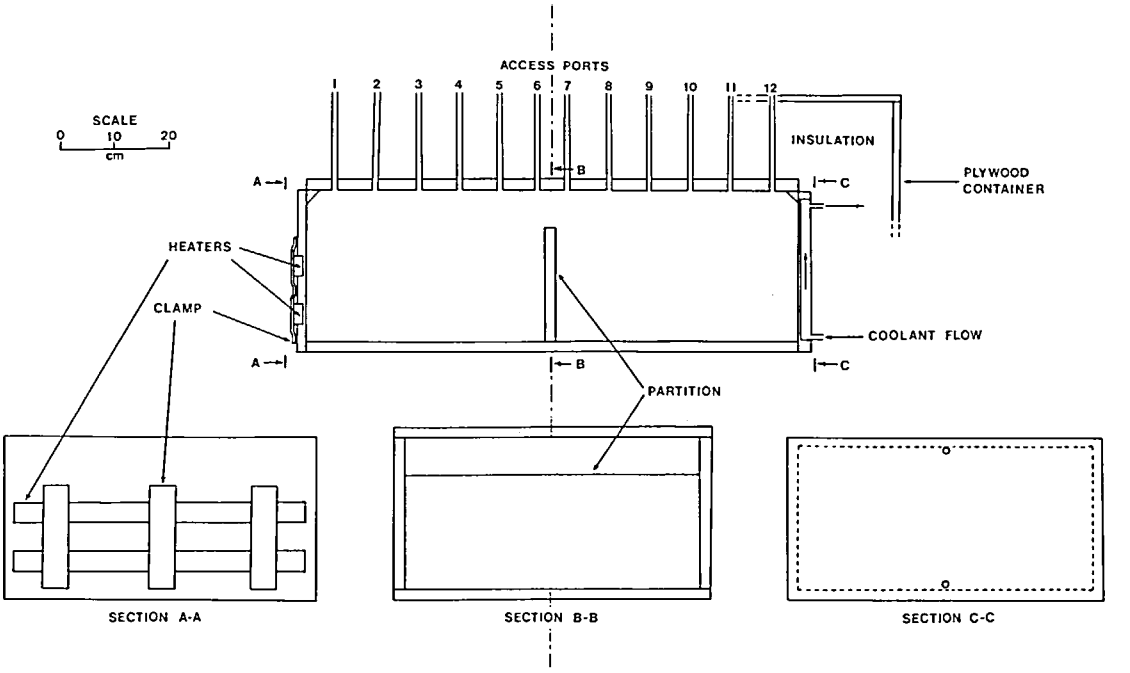

FIG. 2(a). Construction details of the experimental apparatus.

aperture range not examined in ref. [6], namely, $1/4 < Ap < 0$;

(4) measure the heat transfer impact of a 'non-conducting' partition, bearing in mind that the two partition designs in ref. [6] were partially conducting;

(5) correlate the old and the new heat transfer data in a theoretically meaningful way;

(6) determine the temperature and flow fields in the limit of vanishing Rayleigh number, as cornerstone solutions to test the validity of future numerical simulations of the phenomenon.

2. EXPERIMENTAL APPARATUS

Figure 2 shows the experimental apparatus used in the present experiments. The water-filled Plexiglas enclosure available from an earlier experiment [9] was fitted with vertical incomplete partitions designed to be 'non-conducting' relative to the fluid medium (water). As shown in the detail drawing of Fig. 2(b), the partitions were made out of double-wall Plexiglas filled with air. Five different partition heights or apertures were used, $Ap = h/H = 1$ (no partition), 1/4, 1/8, 1/16 and 0 (complete partition).

As in refs. [5, 6], water was used as the convective medium in order to simulate the high Rayleigh numbers characteristic of life-size rooms filled with air. The overall temperature difference between the vertical end plates ranged from 2 to 26°C, yielding Rayleigh numbers based on enclosure height (H) in the range 10^9–10^{10}.

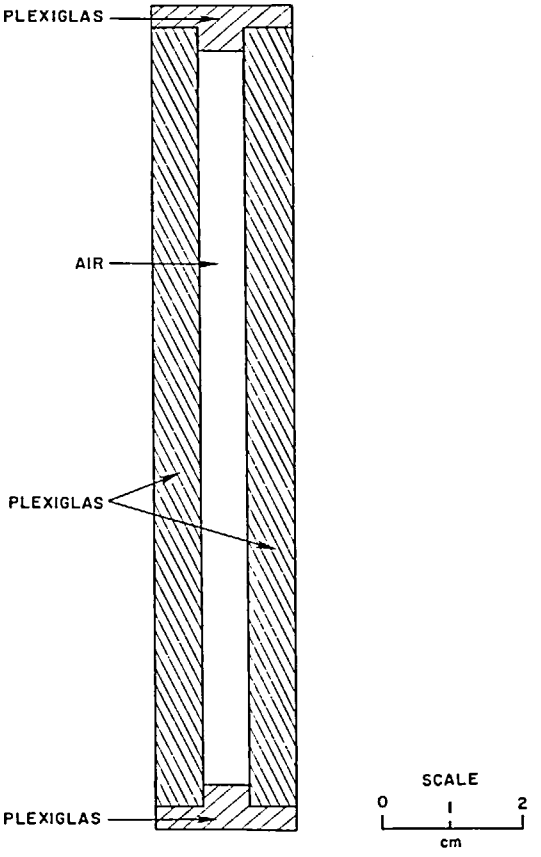

FIG. 2(b). Cross-section through the 'air-gap' partition.

Construction details of the apparatus are given in Fig. 2(a) and in ref. [9]. The four main components of the apparatus are: the Plexiglas box, the partition, the fiberglass insulation, and around everything, the wooden container. The Plexiglas box is made out of 1.9 cm thick Plexiglas sheet; its dimensions are $H = 27.9$ cm, $L = 91.4$ cm and, perpendicular to the plane of Figs. 1 and 2, $W = 54.6$ cm. The box was insulated with 15 cm thick fiberglass supported by the plywood container.

The differentially-heated vertical ends of the box are made out of 1.9 cm thick aluminum plate. The cold end was hollowed out to serve as a heat exchanger and connected to a constant-temperature-bath refrigerator capable of controlling the coolant temperature to within ± 0.1°C. The hot end plate contained two 500 W strip heaters, connected in parallel and recessed into the aluminum plate. All aluminum surfaces were coated with a thin layer of lacquer to inhibit oxidation. A constant-voltage transformer was used to limit the effects of diurnal variations in the building's electrical supply. Total power inputs varied from 10 to 400 W (66–2626 W m^{-2}).

Four partitions of different heights were fabricated from Plexiglas and were mounted in the center of the enclosure on the floor. The partition heights were 20.9, 24.4, 26.2 and 27.9 cm. All the partitions were 1.3 cm thick and contained a 0.64 cm thick layer of air.

Temperature measurements were made to within ± 0.5°C, using type K (chromel–alumel) thermocouples. The end plate temperatures and the ambient temperature were monitored throughout each experiment. In general, it took the apparatus about 24 h to stabilize whenever the power and refrigerator setting were changed. Arrival at steady-state was determined by monitoring the end plate temperature. When steady-state was achieved, the experiment was run for approximately 5 h with readings taken every 18 or 30 min. The power input was measured by monitoring heat voltage and current, and varied a maximum of 2%. To minimize the thermal interaction of the apparatus with its surroundings, the hot wall temperature and cold wall temperature were carefully adjusted so that the mean operating temperature, $(T_H + T_C)/2$, was within ± 5°C of ambient.

3. VELOCITY MEASUREMENTS

The flow was made visible using the thymol blue pH-indicator technique originally described by Baker [10] and used extensively in water natural convection experiments (see, for example, refs. [11–14]). Two wire electrodes were inserted into the pH-neutral (tea colored) flow; with 6 V between the electrodes, the cathode marked the flow by causing a local pH and color change towards deep blue. As shown by the sequence of photographs in Fig. 3, the time evolution of

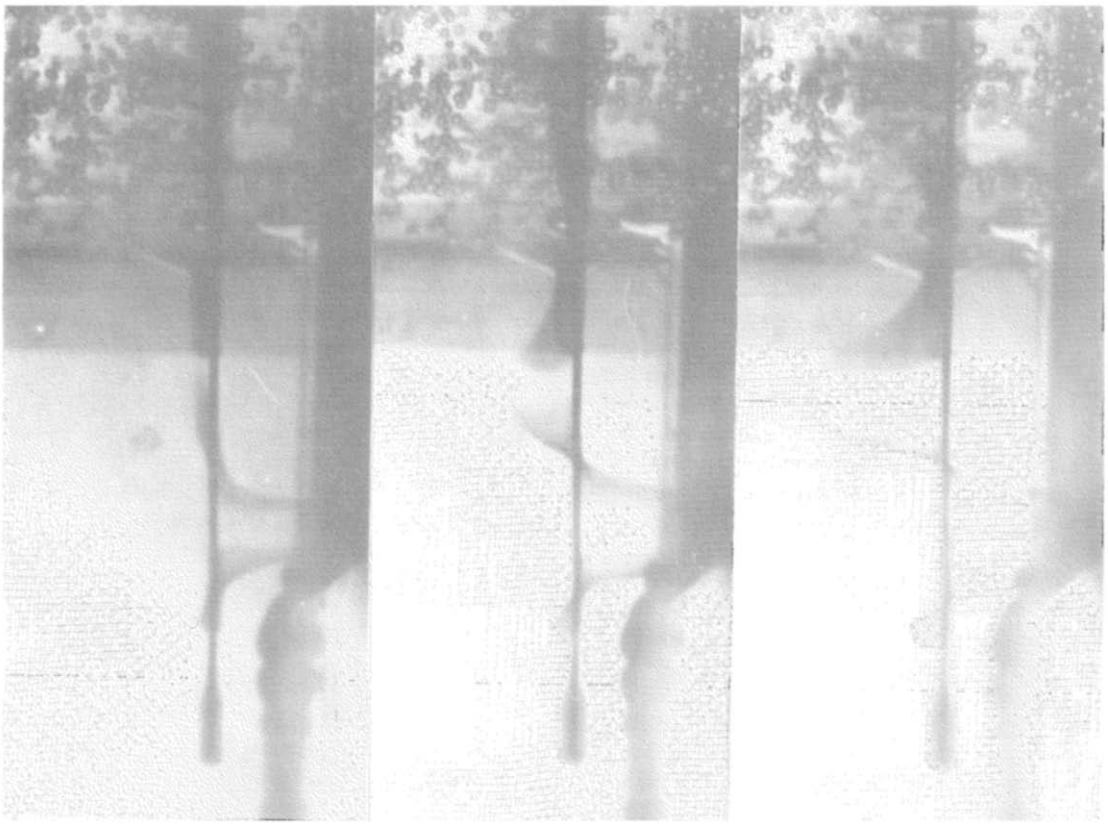

FIG. 3. Flow visualization on the cold side of the partition, $Ap = 1/4$, $Ra_H = 9.2 \times 10^9$; from left to right, $t = 36$, 54 and 75 s.

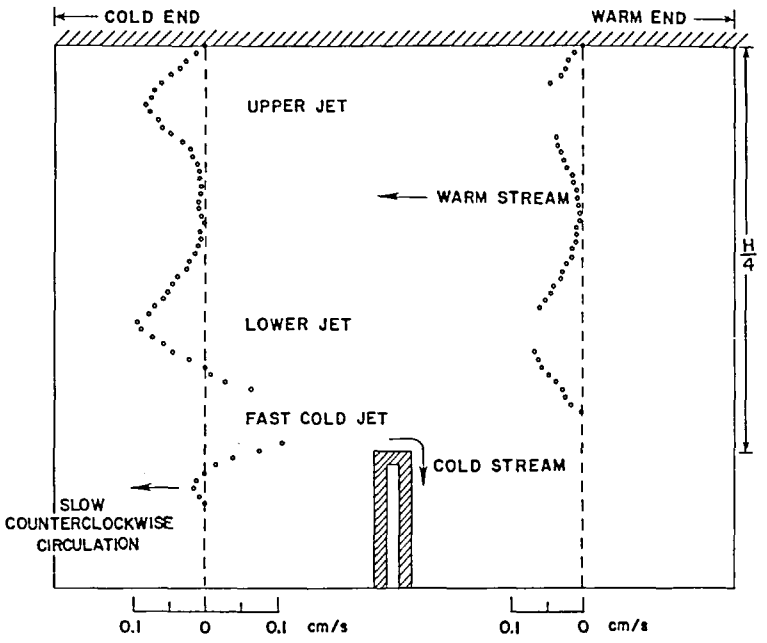

FIG. 4(a). Horizontal velocity profile near the aperture ($Ap = 1/4, Ra_H = 9.2 \times 10^9, Nu = 30.6$); the dashed line represents the position of the electrode.

the marked fluid was used in order to calculate the fluid velocity [15].

Velocity measurements were performed in two distinct cases, $Ap = 1/4$ and $1/8$, as shown in Figs. 4(a) and (b). Drawn to scale on these figures is the geometry of the aperture region and the relative position of the vertical wire (cathode) responsible for the horizontal velocity profiles shown. Looking at the 'wide' aperture case [Fig. 4(a)] and keeping in mind that heating is provided from the right (Fig. 1), above the divider we see a counterflow in which cold fluid flows very fast (0.5 cm s^{-1}) as a thin jet and falls over the top of the partition into the warm chamber, while warm fluid takes its place by moving slowly from right to left. We were unable to measure the cold jet peak velocity using the thymol blue method. The counterflow of Fig. 4(a) was described qualitatively in ref. [6], however, unlike in ref. [6] we find that the thicker branch of the counterflow has two velocity maxima. These two horizontal jets are visualized by the velocity profiles on both sides of the vertical plane of the aperture. The upper jet appears to be the continuation of the warm jet driven upwards along the heated wall of the box, while the lower jet is induced by the fast cold jet, in the manner of a

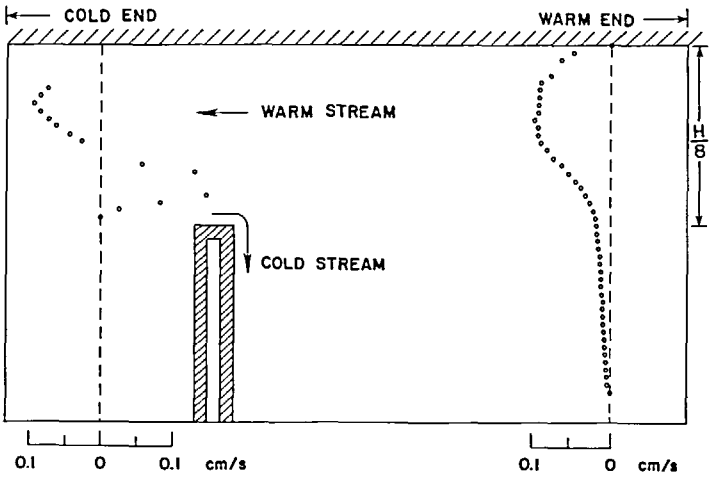

FIG. 4(b). Horizontal velocity profile near the aperture ($Ap = 1/8, Ra_H = 1.05 \times 10^{10}, Nu = 18.5$); the dashed line represents the position of the electrode. The peak velocity of the cold jet falling over the partition is of the order of 0.5 cm s^{-1}.

horizontal jet in a thermally stratified pool [16]. The lower section of the velocity profile on the cold (left) side of the partition in Fig. 4(a) is very similar to the parallel opposing jets observed in shallow enclosures at high Rayleigh numbers [17].

Figure 4(b) shows that as the aperture shrinks to $Ap = 1/8$, the warm (upper) stream exhibits a single velocity maximum, as if the two warm jets of Fig. 4(a) have been forced to merge.

4. HEAT TRANSFER RESULTS

The net heat transfer rate across the enclosure was measured electrically, by monitoring the power dissipated in the warm plate resistors [Fig. 2(a)]. The heat transfer measurements are presented in Fig. 5, where the Nusselt number and Rayleigh number are defined as follows:

$$Nu = \frac{Q/W}{k(T_H - T_C)}, \tag{1}$$

$$Ra_H = \frac{g\beta H^3(T_H - T_C)}{\alpha\nu}. \tag{2}$$

The physical properties appearing in the above definitions have been evaluated at the end-to-end average temperature $(T_H + T_C)/2$. Note also that, unlike in ref. [6] where the Rayleigh number is based on the horizontal dimension of the enclosure, in equation (2) the Rayleigh number is based on height.

Figure 5 shows that the heat transfer rate decreases drastically as the aperture ratio Ap decreases from $Ap = 1$ (no partition) to $Ap = 0$ (complete partition): over this range, the Nusselt number decreases by a factor of 15 which is approximately the ratio between the thermal conductivities of water and air (this particular measurement verifies the effectiveness of the 'air-gap' design as a 'non-conducting' partition, Fig. 2(b), stating that in the full-partition case ($Ap = 0$) the thermal resistance is dominated by the air gap).

Figure 5 shows also the heat transfer data published earlier by Nansteel and Greif [6] using a partition built out of polystyrene sandwiched between stainless steel sheets. Compared with the present measurements, the Nansteel and Greif data document only the large aperture range, $1 \geqslant Ap \geqslant 1/4$. However, two sets of data reported by Nansteel and Greif ($Ap = 1$ and $1/4$) can be compared directly with the corresponding data yielded by the present measurements: the heat transfer rate reported by Nansteel and Greif is generally 50% larger than the value yielded by the present experiments. In addition, the drop in Nu from $Ap = 1$ to $1/4$ in the Nansteel and Greif data is less than the corresponding drop exhibited by the present measurements: this apparent discrepancy can be attributed to the fact that the present partition is a better insulator than the 'non-conducting' partition used in ref. [6].

To shed more light on the 50% discrepancy between the present Nu data and those of ref. [6], Fig. 6 shows a compilation of all the high-Rayleigh number data obtained in horizontal enclosures heated from the side (no partition, $Ap = 1$). Both ref. [6] and the present measurements extend the Ra_H domain in which the heat transfer rate has been known experimentally [17].

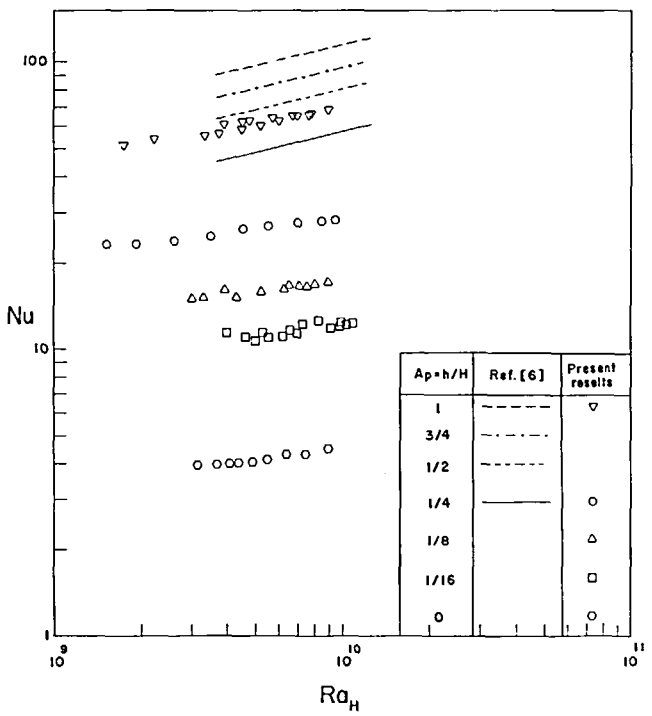

FIG. 5. The effect of aperture ratio ($Ap = h/H$) on the net heat transfer (see also Table 1).

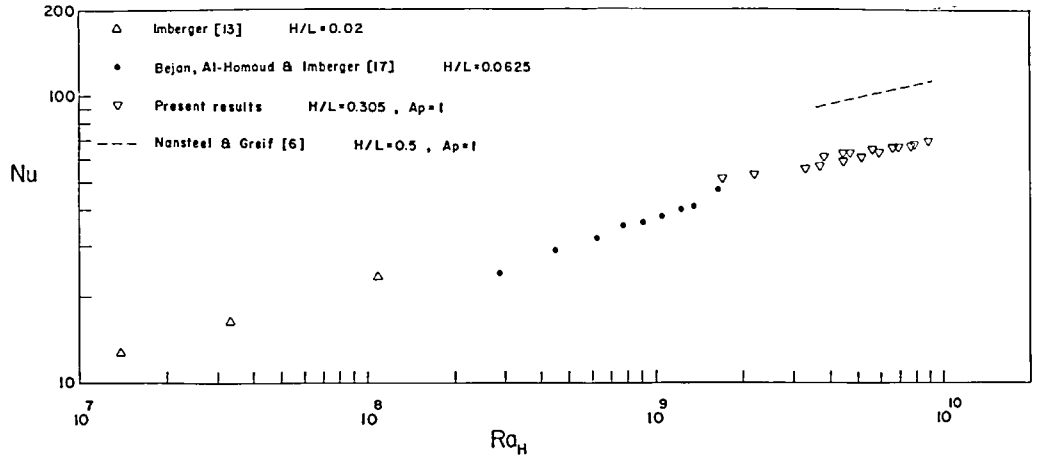

FIG. 6. Summary of high Ra_H heat transfer measurement in a shallow enclosure heated in the end-to-end direction.

However, as the enclosure aspect ratio H/L does not seem to have a significant effect on the Nu–Ra_H relationship, the $Ap = 1$ data of Nansteel and Greif [6] fall above what seems to be a general Nu–Ra_H curve in the high Ra_H limit. A possible explanation for the 50% discrepancy between the $Ap = 1$ sets of data is that, with an aspect ratio $H/L = 0.5$, the enclosure of ref. [6] departs sufficiently from the behavior of 'shallow' enclosures ($H/L \ll 1$). Another explanation is that in ref. [6] the heat transfer rate was measured via the enthalpy drop experienced by the stream that heated the warm end of the enclosure, whereas in the present experiment the heat input was measured directly (electrically). Furthermore, the insulation heat leak evaluated in ref. [6] appears to account for a higher percentage of the end-to-end heat transfer rate than in the present experiment, where it was less than 10% (see also ref. [9]).

5. HEAT TRANSFER CORRELATION

The strong heat transfer effect of opening the aperture Ap, documented here and in ref. [6], can be predicted based on scale analysis. Focusing on the basic heat transfer geometry shown in Fig. 1, the convective heat transfer from T_H to T_C overcomes two thermal resistances in series. The first resistance is the thermal boundary layer lining the entire hot wall

$$R_H \sim \frac{H\, Ra_H^{-1/4}}{k(HW)}, \tag{3}$$

where $H\, Ra_H^{-1/4}$ is the scale of the thermal boundary layer thickness and HW the area of the hot wall covered by the thermal boundary layer. The second resistance is the thermal boundary layer along the top portion of the cold wall, where the strong convective cell makes contact with the heat sink

$$R_C \sim \frac{h\, Ra_h^{-1/4}}{k(hW)}. \tag{4}$$

In an order of magnitude sense, the net heat transfer rate Q is

$$Q \sim \frac{\Delta T}{R_H + R_C}, \tag{5}$$

in other words, using equations (3) and (4)

$$Nu = B_1 \frac{Ra_H^{1/4}}{Ap^{-3/4} + B_2}, \tag{6}$$

where B_1 and B_2 are numerical constants of order one. Figure 7 shows that the data of Fig. 5 are correlated reasonably well by taking $B_2 = 0.5$; the projection of these data on Fig. 7 suggests that the value of the leading coefficient B_1 is approximately 0.336. In conclusion, the expression

$$Nu = 0.336 \frac{Ra_H^{1/4}}{Ap^{-3/4} + 0.5}, \tag{7}$$

correlates the present data for a non-conducting partition in the range $1 < Ap < 1/16$. The standard deviation of the experimental data from curve (7) is 7.2%. The Nansteel and Greif data of Fig. 5 are correlated by an expression similar to equation (7) where the coefficient 0.336 is replaced by 0.56 with the standard deviation of 5.8%.

6. THE LOW RAYLEIGH NUMBER LIMIT

The object of the experimental study described above has been the high Rayleigh number regime in which the enclosure heat transfer is dominated by convective effects. More insight into the phenomenon is gained by invoking the low Rayleigh number or conduction-dominated limit. An analytical understanding of this limit is very useful in assessing the validity of numerical simulations of finite-Ra_H situations [8]. Furthermore, many spacecraft applications of the geometry of Fig. 1 operate under 'near $g = 0$' conditions, hence in the $Ra_H \to 0$ limit. The purpose of this last section is to re-

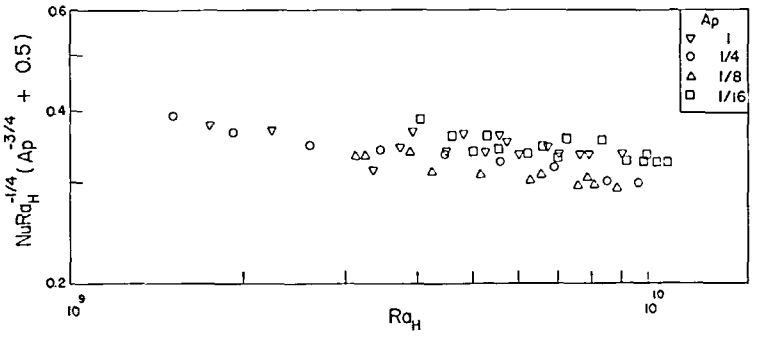

FIG. 7. Heat transfer correlation for natural convection in an enclosure with partial non-conducting vertical partition (see also Table 1).

port a perturbation solution for the flow and temperature field in the low Rayleigh number regime. In view of the small Rayleigh number, the perturbation solution is not relevant to the high-Ra_H picture revealed by the experiment of Sections 2–5.

6.1. *Mathematical formulation*

Consider the two-dimensional geometry of Fig. 1 and a Cartesian system x–y such that the x axis is oriented horizontally. In that system, the equations accounting for the conservation of mass, momentum and energy are

$$\frac{\partial u}{\partial x}+\frac{\partial v}{\partial y}=0, \tag{8}$$

$$u\frac{\partial \zeta}{\partial x}+v\frac{\partial \zeta}{\partial y}=\nu\left(\frac{\partial^2\zeta}{\partial x^2}+\frac{\partial^2\zeta}{\partial y^2}\right)+\beta g\frac{\partial T}{\partial x}, \tag{9}$$

$$u\frac{\partial T}{\partial x}+v\frac{\partial T}{\partial y}=\alpha\left(\frac{\partial^2 T}{\partial x^2}+\frac{\partial^2 T}{\partial y^2}\right), \tag{10}$$

where

$$\zeta=-\left(\frac{\partial^2\psi}{\partial x^2}+\frac{\partial^2\psi}{\partial y^2}\right), \tag{11}$$

$$u=\frac{\partial\psi}{\partial y},\quad v=-\frac{\partial\psi}{\partial x}. \tag{12}$$

In equations (8)–(12), u, v, ζ and ψ are the horizontal velocity, vertical velocity, vorticity function and stream function, respectively. The fluid filling the cavity has been modeled as Newtonian; in addition, the fluid is assumed to conform to the Boussinesq approximation whereby the density varies linearly with temperature in the body force term of equation (9).

Non-dimensionalization is achieved by defining the new dimensionless variables

$$X=\frac{x}{L},\quad Y=\frac{y}{L},\quad \theta=\frac{T-T_C}{T_H-T_C},$$
$$\Psi=\frac{\psi}{\beta g L^3(T_H-T_C)/\nu},\quad Z=\frac{\zeta}{\beta g L(T_H-T_C)/\nu}. \tag{13}$$

The dimensionless forms of the governing equations are then

$$\frac{Ra_L}{Pr}\left(\frac{\partial\Psi}{\partial Y}\frac{\partial Z}{\partial X}-\frac{\partial\Psi}{\partial X}\frac{\partial Z}{\partial Y}\right)=\frac{\partial^2 Z}{\partial X^2}+\frac{\partial^2 Z}{\partial Y^2}+\frac{\partial\theta}{\partial X}, \tag{14}$$

$$Ra_L\left(\frac{\partial\Psi}{\partial Y}\frac{\partial\theta}{\partial X}-\frac{\partial\Psi}{\partial X}\frac{\partial\theta}{\partial Y}\right)=\frac{\partial^2\theta}{\partial X^2}+\frac{\partial^2\theta}{\partial Y^2}, \tag{15}$$

with

$$Z=-\left(\frac{\partial^2\Psi}{\partial X^2}+\frac{\partial^2\Psi}{\partial Y^2}\right). \tag{16}$$

Unlike in the presentation of heat transfer measurements [Figs. 4–6, equation (2)], this time the Rayleigh number Ra_L is based on the horizontal dimension of the overall cavity

$$Ra_L=\frac{g\beta L^3(T_H-T_C)}{\alpha\nu}. \tag{17}$$

Finally, the boundary conditions for the partially divided enclosure of Fig. 1 are

$$\begin{aligned}
&\text{at } X=0: && \Psi=0,\ \frac{\partial\Psi}{\partial X}=0, && \theta=0,\\
&\text{at } X=1: && \Psi=0,\ \frac{\partial\Psi}{\partial X}=0, && \theta=1,\\
&\text{at } Y=0,\frac{H}{L}: && \Psi=0,\ \frac{\partial\Psi}{\partial Y}=0, && \frac{\partial\theta}{\partial Y}=0,\\
&\text{at } X=1/2,\\
&\text{and } 0\leqslant Y\leqslant\frac{H-h}{L}: && \Psi=0,\ \frac{\partial\Psi}{\partial X}=0, && \frac{\partial\theta}{\partial X}=0.
\end{aligned} \tag{18}$$

6.2. *Asymptotic expansion*

Regarding the Rayleigh number as a small enough parameter, we seek series solutions of the following form

$$\begin{aligned}
\theta&=\theta_0+Ra_L\,\theta_1+Ra_L^2\,\theta_2+\cdots\\
Z&=Z_0+Ra_L\,Z_1+Ra_L^2\,Z_2+\cdots\\
\Psi&=\Psi_0+Ra_L\,\Psi_1+Ra_L^2\,\Psi_2+\cdots
\end{aligned} \tag{19}$$

Table 1. Heat transfer measurements

Ap	$Ra_H \times 10^9$	Nu	$Nu\, Ra_H^{-1/4}\,(Ap^{-3/4}+0.5)$
	1.74	51.17	0.376
	2.24	53.51	0.369
	3.38	50.71	0.315
	3.74	56.72	0.344
	3.92	61.11	0.366
	4.50	58.54	0.339
	4.56	62.36	0.360
	4.82	63.68	0.363
1	5.24	60.65	0.338
	5.73	64.41	0.351
	6.01	62.43	0.336
	6.72	65.93	0.345
	7.03	65.21	0.338
	7.68	66.05	0.335
	7.90	66.51	0.335
	9.03	68.85	0.335
	1.50	23.15	0.391
	1.92	22.92	0.364
	2.59	23.61	0.348
1/4	3.48	24.86	0.341
	4.48	26.07	0.335
	5.58	26.80	0.326
	6.90	27.62	0.319
	8.52	27.60	0.302
	9.63	23.03	0.298
	3.14	14.95	0.332
	3.26	15.10	0.332
	3.93	16.10	0.338
	4.26	15.21	0.313
	5.19	15.74	0.308
1/8	6.31	16.16	0.301
	6.46	16.67	0.309
	7.09	16.73	0.303
	7.60	16.52	0.294
	8.05	16.85	0.296
	8.915	16.99	0.291
	4.04	11.47	0.387
	4.66	11.04	0.359
	5.03	10.63	0.339
	5.30	11.48	0.362
	5.55	10.99	0.342
	6.26	11.12	0.336
	6.59	11.59	0.346
1/16	7.01	11.29	0.332
	7.26	12.26	0.357
	8.39	12.58	0.353
	9.19	11.89	0.326
	9.86	12.09	0.326
	9.96	12.42	0.334
	10.40	12.16	0.324
	10.96	12.35	0.324

Substituting these expressions into equations (14) and (15), collecting the terms containing the same power of Ra_L and setting such groups equal to zero, yields a sequence of problems, one for each power of Ra_L.

The zero-order flow and temperature field (θ_0, Ψ_0), which is valid strictly in the limit $Ra_L \to 0$ obeys the following system

$$0 = \frac{\partial^2 \theta_0}{\partial X^2} + \frac{\partial^2 \theta_0}{\partial Y^2}, \tag{20}$$

$$0 = \frac{\partial^2 Z_0}{\partial X^2} + \frac{\partial^2 Z_0}{\partial Y^2} + \frac{\partial \theta_0}{\partial X}, \quad Z_0 = -\nabla^2 \Psi_0, \tag{21}$$

subject to boundary conditions of type (18). This system was solved numerically, as discussed later in this section. With θ_0 and Ψ_0 calculated numerically, the first-order fields (θ_1, Ψ_1) are obtained next by solving the system

$$\frac{\partial \Psi_0}{\partial Y}\frac{\partial \theta_0}{\partial X} - \frac{\partial \Psi_0}{\partial X}\frac{\partial \theta_0}{\partial Y} = \frac{\partial^2 \theta_1}{\partial X^2} + \frac{\partial^2 \theta_1}{\partial Y^2}, \tag{22}$$

$$\frac{1}{Pr}\left(\frac{\partial \Psi_0}{\partial Y}\frac{\partial Z_0}{\partial X} - \frac{\partial \Psi_0}{\partial X}\frac{\partial Z_0}{\partial Y}\right) = \frac{\partial^2 Z_1}{\partial X^2} + \frac{\partial^2 Z_1}{\partial Y^2} + \frac{\partial \theta_1}{\partial X},$$

$$Z_1 = -\nabla^2 \Psi_1. \tag{23}$$

6.3. *Results*

The asymptotic solution (θ_0, Ψ_0) and its first correction (θ_1, Ψ_1) were obtained based on a finite-difference approximation of the governing equations. The computer program used in this part of the study is listed in a thesis by Lin [18]. Initial guesses for temperature, vorticity and stream function were updated (improved) using the successive overrelaxation scheme until the following convergence criterion was satisfied

$$\frac{\sum_m \sum_n |\phi^k(m,n) - \phi^{k-1}(m,n)|}{\sum_m \sum_n \phi^{k-1}(m,n)} < 10^{-5}. \tag{24}$$

In the above criterion ϕ stands for θ, Ψ or Z, and m, n and k for node coordinates and order of iteration. All calculations displayed here were made using $m = 22$, $n = 11$, $H/L = 1/2$ and $Pr = 0.71$ (permanent gases).

Figures 8(a) and (b) and Table 2 show the results of solving problems (20), (21) and (22), (23) numerically. The isotherms and streamlines of Fig. 8(a) demonstrate that in the $Ra_L \to 0$ limit the pure conduction temperature distribution drives a counterclockwise symmetric circulation in which the fluid rises along the heated wall. When the aperture is relatively open ($Ap = 0.7$) the flow consists of a single cell, as the two sides of the cavity exchange fluid very effectively through the aperture. As the aperture ratio Ap decreases, the flow is reduced and severed into two

Table 2. Principal numerical values of the zero and first-order solutions in the $Ra_L \to 0$ limit ($Pr = 0.71$, $H/L = 1/2$)

Function		$Ap = 0.7$	$Ap = 0.5$	$Ap = 0.3$
θ_0	max	1	1	1
	min	0	0	0
Ψ_0	max	0	0	0
	min	-1.018×10^{-3}	-6.51×10^{-4}	-4.31×10^{-4}
θ_1	max	6.55×10^{-5}	3.27×10^{-5}	1.76×10^{-5}
	min	-1.25×10^{-4}	-5.22×10^{-5}	-1.87×10^{-5}
Ψ_1	max	3.05×10^{-8}	3.02×10^{-8}	2.66×10^{-8}
	min	-3.05×10^{-8}	-3.02×10^{-8}	-2.66×10^{-8}

[LHS of each Ψ_1 plot in Fig. 8(b)]

$\Psi > 0$: clockwise circulation.
$\Psi < 0$: counterclockwise circulation.

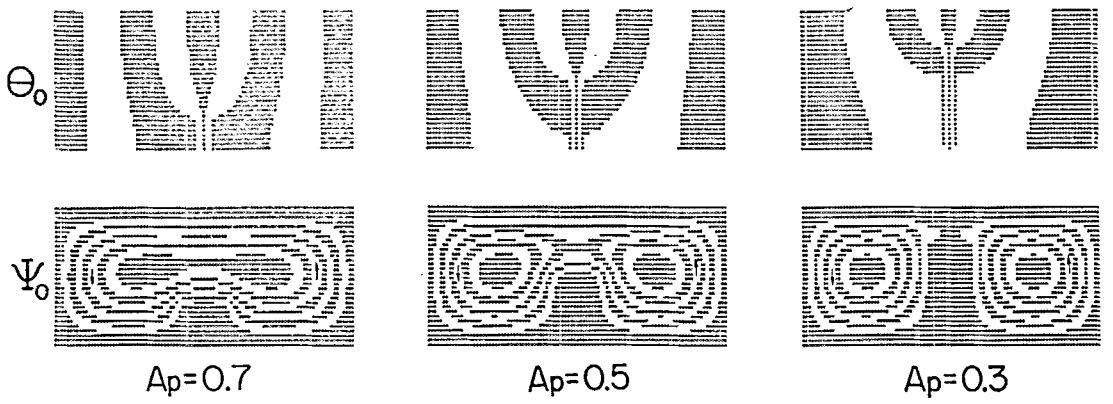

FIG. 8(a) The zero-order temperature and flow fields, θ_0, ψ_0.

counterclockwise cells. The first-order correction to the temperature field, Fig. 8(b), amounts to a vertical thermal stratification of the fluid. The first-order correction to the streamline pattern has the effect of pushing the streamlines closer to the vertical differentially-heated walls, suggesting a gradual approach to the boundary layer regime as Ra_L increases.

7. CONCLUSIONS

This paper described an experimental and numerical study of the phenomenon of natural convection in a partially divided enclosure heated from the side. The experimental part of the study led to the following conclusions:

(1) The flow field in the high Rayleigh number regime is characterized by boundary layer upflow along the heated wall, horizontal counterflow through the aperture and trapped fluid on the lower cold side of the partition (Fig. 1). These features confirm those described in earlier studies [5–7]. An additional characteristic of the flow is the presence of two velocity maxima in the warm stream of the aperture counterflow when the aperture is 'large' [Fig. 4(a)]. As the aperture closes, the warm stream attains a single velocity maximum [Fig. 4(b)].

(2) Heat transfer measurements in the 'small' aperture range not studied previously ($Ap < 1/4$) demonstrate that the partial wall reduces significantly the net heat transfer between the ends of the cavity (Fig. 5). The present 'air-gap' design of the partition has been proved effective in avoiding the heat transfer directly through the partition.

(3) The present heat transfer measurements are generally 50% lower than earlier results published for $Ap = 1, 1/4$ [6], Figs. 5 and 6. The discrepancy may be attributed to three-dimensional effects, or to different degrees of heat leakage through all lateral walls.

(4) The heat transfer data are correlated satisfactorily by equation (7), Fig. 7, which is based on recognizing the proper thermal resistance scales of the phenomenon.

The numerical part of the study focused on the $Ra_L \to 0$ limit, in which it is possible to determine the flow as an asymptotic expansion in 'Ra_L small'. The temperature and flow fields are displayed in Figs. 8(a) and (b), and their numerical characteristics are summarized in Table 2. In the conduction-dominated limit the flow is symmetric with counterflow exchange

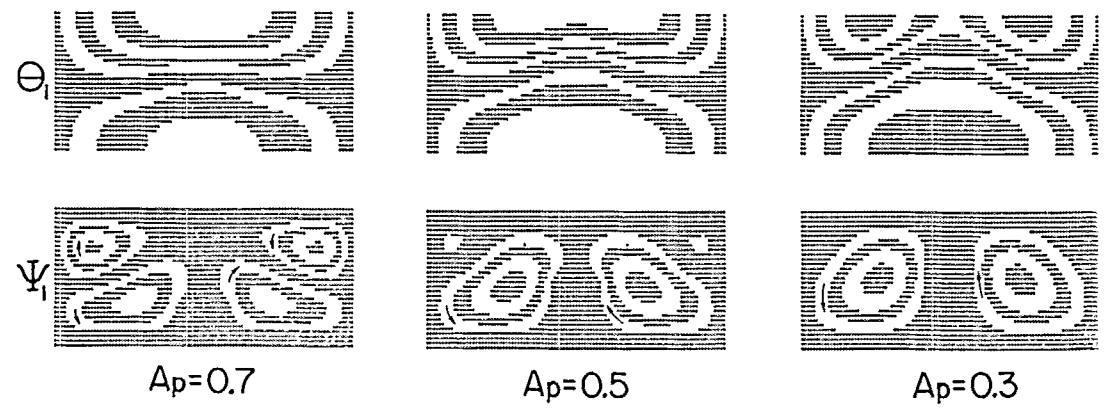

FIG. 8(b). The first-order corrections to the temperature and flow fields, θ_1, ψ_1.

rough the aperture [Fig. 8(a)]. As Ra_L increases, the nd boundary layers become thinner, while the fluid roughout the cavity becomes thermally stratified Fig. 8(b)].

cknowledgements—N. N. Lin wishes to acknowledge the nancial support received from Taiwan, China, in the form of a raduate Fellowship. The apparatus was designed by Mr Ren nderson for an earlier research project [9]. The apparatus as constructed by Mr Karl Rupp and Mr Michael Hacker nd the instrumentation by Mr Richard Cowgill.

REFERENCES

1. I. Catton, Natural convection in enclosures, *Proc. 6th Int. Heat Transfer Conf.*, Vol. 6, pp. 13–43. Toronto (1979).
2. Y. Jaluria, *Natural Convection Heat and Mass Transfer*, pp. 209–235. Pergamon Press, Oxford (1980).
3. S. Ostrach, Natural convection in enclosures, *Adv. Heat Transfer* **8**, 161–227 (1972).
4. K. T. Yang and J. R. Lloyd, *Proc. Workshop on Natural Convection*. Breckenridge, Colorado, 18–21 July (1982); sponsored by National Science Foundation and University of Notre Dame.
5. A. Bejan and A. N. Rossie, Natural convection in horizontal duct connecting two fluid reservoirs, *J. Heat Transfer* **103**, 108–113 (1981).
6. M. W. Nansteel and R. Greif, Natural convection in undivided and partially divided rectangular enclosures, *J. Heat Transfer* **103**, 623–629 (1981).
7. S. M. Bajorek and J. R. Lloyd, Experimental investigation of natural convection in partitioned enclosures, *J. Heat Transfer* **104**, 527–532 (1982).
8. A. Gadgil, Comments during the *Natural Convection Workshop* (see ref. [4]).
9. R. Anderson and A. Bejan, Heat transfer through single and double vertical walls in natural convection: theory and experiments, *Int. J. Heat Mass Transfer* **24**, 1611–1620 (1981).
10. D. J. Baker, A technique for the precise measurement of small fluid velocities, *J. Fluid Mech.* **26**(3), 573–575 (1966).
11. E. M. Sparrow, R. B. Husar and R. J. Goldstein, Observations and other characteristics of thermals, *J. Fluid Mech.* **41**, 793–800 (1970).
12. R. Eichhorn, J. H. Lienhard and C. C. Chen, Natural convection from isothermal spheres and cylinders, *Proc. 5th Int. Heat Transfer Conf.*, Paper NC1.3. Tokyo (1974).
13. J. Imberger, Natural convection in a shallow cavity with differentially heated end walls. Part 3. Experimental results, *J. Fluid Mech.* **65**(2), 247–260 (1974).
14. A. Bejan and R. B. Yewell, The effect of hydrogen bubbles on the thymol blue velocity measurement technique, *Int. J. Heat Fluid Flow* **2**(4), 201–204 (1980).
15. A. Bejan and S. Kimura, Penetration of free convection into a lateral cavity, *J. Fluid Mech.* **103**, 465–478 (1981).
16. J. Imberger, R. Thompson and C. Fandry, Selective withdrawal from a finite rectangular tank, *J. Fluid Mech.* **78**, 489–512 (1976).
17. A. Bejan, A. A. Al-Homoud and J. Imberger, Experimental study of high-Rayleigh-number convection in a horizontal cavity with different end temperatures, *J. Fluid Mech.* **109**, 283–299 (1981).
18. N. N. Lin, Natural convection in partially divided enclosures, M.S. Thesis, Department of Mechanical Engineering, University of Colorado, Boulder, Colorado, December (1982).

CONVECTION NATURELLE DANS UNE ENCEINTE PARTIELLEMENT DIVISEE

Résumé—On décrit une étude expérimentale et analytique du phénomène de transfert thermique par convection naturelle dans une enceinte rectangulaire munie d'une cloison interne incomplète. Les expériences sont conduites avec une enceinte remplie d'eau avec des parois horizontales adiabatiques et des parois verticales maintenues à des températures différentes. Les mesures de transfert thermique et les visualisations d'écoulement correspondent à un domaine de nombre de Rayleigh 10^9–10^{10}, à des rapports d'ouverture $h/H = 1, 1/4, 1/8, 1/16$ et 0 où h et H sont la hauteur de l'ouverture interne (au-dessus de la partition) et la hauteur de l'enceinte. On montre que le rapport d'ouverture h/H a un effet important à la fois sur le transfert de chaleur et la configuration de l'écoulement. Le seconde partie de l'étude consiste en une analyse asymptotique du même phénomène, valable dans la limite des très faibles nombres de Rayleigh. Les champs de vitesse et de température sont dans ce cas donnés graphiquement pour $H/L = 0{,}5$, $Pr = 0{,}71$ et $0{,}3 < h/H < 0{,}7$, avec L et Pr respectivement la longueur de l'enceinte et le nombre de Prandtl.

NATÜRLICHE KONVEKTION IN EINEM PARTIELL UNTERTEILTEN HOHLRAUM

Zusammenfassung—Die vorliegende Arbeit beschreibt eine experimentelle und analytische Untersuchung der Wärmeübertragung durch natürliche Konvektion in einem rechteckigen Hohlraum, dessen Inneres unvollständig aufgeteilt ist. Die Versuche wurden in einem wassergefüllten Hohlraum durchgeführt, dessen horizontale Wände adiabat sind und dessen senkrechte Wände unterschiedliche Temperaturen haben. Messungen des Wärmeüberganges und Untersuchungen mit sichtbar gemachter Strömung wurden durchgeführt bei Rayleigh-Zahlen zwischen 10^9 und 10^{10}, bei Öffnungsverhältnissen $h/H = 1, 1/4, 1/8, 1/16$ und 0, wobei h die lichte Höhe der inneren Öffnung und H die innere Gesamthöhe ist. Es wird gezeigt, daß das Öffnungsverhältnis h/H einen starken Einfluß auf den Wärmeübergang und auf die Strömungsform ausübt. Der zweite Teil der Untersuchung stellt eine Grenzbetrachtung derselben Erscheinung im Bereich verschwindender Rayleigh-Zahlen dar. Die Geschwindigkeits- und Temperaturfelder in diesem Bereich sind graphisch dargestellt für $H/L = 0{,}5$, $Pr = 0{,}71$ und $0{,}3 < h/H < 0{,}7$, wobei L die Länge des Hohlraumes und Pr die Prandtl-Zahl ist.

ЕСТЕСТВЕННАЯ КОНВЕКЦИЯ В ЧАСТИЧНО ПЕРЕГОРОЖЕННОЙ ПОЛОСТИ

Аннотация—Описывается экспериментальное и аналитическое исследование явления переноса тепла естественной конвекцией в частично перегороженной прямоугольной полости. Эксперименты проводились с заполненной водой полостью, горизонтальные стенки которой были адиабатическими, а вертикальные имели разные температуры. Измерения величины теплового потока и визуализация течения осуществлялись в диапазоне чисел Рэлея 10^9–10^{10} при значениях отношения h/H, равных 1, $\frac{1}{4}$, $\frac{1}{8}$, $\frac{1}{16}$ и 0, где h и H – соответственно высота внутреннего отверстия над перегородкой и высота полости. Показано, что величина h/H оказывает большое влияние как на интенсивность теплопереноса, так и на картину течения. Вторая часть исследования посвящена асимптотическому анализу того же явления, но в пределе исчезающе малых значений числа Рэлея. Поля течений и температур в этом пределе представлены в графическом виде для $H/L = 0{,}5$, $Pr = 0{,}71$ и $0{,}3 < h/H < 0{,}7$, где L и Pr – соответственно длина полости и число Прандтля.